AN ELECTROCHEMICAL AND SURFACE ANALYSIS
STUDY OF THE INFLUENCE OF PHOSPHORUS ON
THE CORROSION OF IRON IN CALCIUM NITRATE

C. F. Windisch Jr.
D. R. Baer
R. H. Jones
M. H. Engelhard

October 1990

Presented at the
178th Meeting of Electrochemical Society
Seattle, Washington
October 14-19, 1990

Pacific Northwest Laboratory
Richland, Washington 99352

MASTER

DISTRIBUTION OF THIS DOCUMENT IS UNLIMITED

Rec'

NOV 1 9 1990

AN ELECTROCHEMICAL AND SURFACE ANALYSIS STUDY OF THE INFLUENCE OF PHOSPHORUS ON THE CORROSION OF IRON IN CALCIUM NITRATE

C. F. Windisch Jr., D. R. Baer, R. H. Jones, and M. H. Engelhard

Pacific Northwest Laboratory, Richland, WA 99352

Abstract

Intergranular stress corrosion cracking (IGSCC) of metallic alloys including iron is strongly influenced by the presence of grain boundary impurities such as phosphorus. In this study to determine how phosphorus affects the corrosion of iron, electrochemical polarization methods were used in conjunction with surface analyses employing ultra-high vacuum transfer. Specifically, these methods were used to examine the corrosion of iron, iron/phosphorus alloys, and iron implanted with phosphorus in deaerated 55 wt% $Ca(NO_3)_2$ solutions at 60°C.

The presence of phosphorus in iron accelerated corrosion in both the active and passive regions, with the effect more pronounced in the passive region. In the active region, the phosphorus was oxidized to phosphate which, in turn, appeared to assist the dissolution of the semi-protective Fe_3O_4. In the passive region, the phosphorus accelerated corrosion by some other mechanism, possibly involving phosphide species. The $FePO_4$ that formed in the passive region did not inhibit passivation but, rather, was incorporated in the passive film. The results were found to be consistent with the high IGSCC rates observed for iron containing phosphorus segregated at grain boundaries.

Introduction

This study of the influence of phosphorus on the electrochemical behavior of iron in calcium nitrate at 60°C is motivated by a series of crack growth measurements on phosphorus- and sulfur-containing iron [1,2] and the desire to understand how impurities influence intergranular stress corrosion cracking (IGSCC). It has been widely observed that the segregation of impurities in grain boundaries plays a significant role in the IGSCC of many metal alloys [1-9]. The way in which these impurities influence IGSCC appears to depend strongly on the type of metal undergoing IGSCC and the composition of the electrolyte, as well as the type and amount of impurities present in grain boundaries.

Effects of sulfur and phosphorus on the IGSCC, and general corrosion behavior of nickel in solutions of nitric and sulfuric acid have been studied extensively by a number of workers (3-7). At passive potentials, the presence of phosphorus causes IGSCC while sulfur does not. The same two elements when present on the surface of nickel have different effects on corrosion behavior which, when taken together, can explain the IGSCC results. For example, sulfur has been found to enhance dissolution of nickel in the active potential region but (when IR-drop corrections are applied) appears not to inhibit passivation in the passive potential region (4). Conversely, phosphorus has been shown to slow corrosion in the active potential region but accelerate corrosion in the passive region (3). The apparently opposite behaviors of sulfur and phosphorus on surfaces have been explained by suggesting that the corrosion-enhancing species in the case of sulfur is a surface-persistent sulfide state, formed at active potentials and oxidized to a more benign sulfate at passive potentials. In the case of phosphorus (3), a lower-oxidation-state hypophosphite has been observed to be passivating, giving a protective barrier layer in the active potential region, but is not observed at higher normally passive potentials where there is considerable dissolution.

Given the variety of reactions involving grain boundary impurities in nickel, it would not be surprising if similar impurities gave varied behavior in iron. The IGSCC tests indicate that both sulfur and phosphorus enhance cracking at passive potentials (2,8). The current tests have been undertaken to examine the corrosion reactions that occur when phosphorus is present at a surface such as would be the case at a crack wall or an interface like a grain boundary. Phosphorus-containing surfaces are used to partially simulate the effect of phosphorus at the grain boundaries of iron. These results, when compared to sulfur studies just under way, will serve to highlight the similarities and differences among the effects of these impurities and to provide mechanistic details and corrosion data to fit into quantitative models of IGSCC.

Recently published data indicate that the presence of phosphorus accelerates corrosion in both the active and passive regions of iron in hot nitrate solutions. Grabke et al. (9) found increased corrosion near the free corrosion potential when phosphorus was present and explained it by proposing that a slightly negatively charged species, "phosphide" or $P^{\delta-}$, was produced under these conditions that impeded the formation of a semi-protective corrosion product film. Failure to determine the presence of phosphide in post-test analysis was attributed to oxidation by nitrate in solution. In the passive region, Grabke et al. (8) also found increased corrosion of iron when phosphorus was present, particularly after an "incubation period."

In this work, pure iron, rapidly solidified iron/phosphorus alloy samples, and iron samples implanted with phosphorus were examined in an effort to characterize further the influence of phosphorus on the corrosion reactions of iron in hot nitrate solutions. In addition to standard electrochemical methods, surface analysis of the samples was performed employing an ultra-high vacuum (UHV) electrochemical cell-to-spectrometer transfer system.

Experimental Procedures

Potentiodynamic and potential-step tests, often in conjunction with surface spectroscopic analysis, were used to examine the corrosion of pure iron and phosphorus-containing iron in deaerated 55 wt% $Ca(NO_3)_2$ solutions at 60°C. The base material used in this study was (99.999%) pure iron obtained from Johnson Matthey Inc.[a] These samples were sanded to 600-grit paper, polished to a 1-μm diamond finish, and vacuum annealed to remove surface damage. Some of the prepared specimens were sent to Implant Sciences[b] to be implanted with phosphorus using a 125-keV phosphorus ion beam to a dose of 5×10^{16} at·cm^{-2}. (These samples are hereafter referred to as P-implanted samples.) As shown in Fig. 1, the implantation resulted in about a 6.4 at.% maximum concentration of phosphorus in the outer 160 nm of the material. Rapidly solidified amorphous iron alloy samples containing 15 at.% phosphorus were obtained from Battelle Memorial Institute.[c] These specimens (hereafter designated Fe-15P) were in the form of thin ribbons. The electrolyte solution was prepared by dissolving an appropriate amount of reagent-grade $Ca(NO_3)_2$[d] in deionized water to give 55 wt%. About 0.7 L of solution was used for each test. After transferring it to the corrosion cell, the solution was sparged with argon or nitrogen gas for about 1 hour and heated to 60°C. For one series of experiments, NaH_2PO_4 was added to the nitrate solution until it was saturated.

Electrochemical polarization tests were performed using either a PAR[e] 173 or 273 potentiostat. Potentiodynamic scans were performed at 1 mV·s^{-1}. Potential-step current responses were recorded for various times with a strip chart recorder or on computer disk with the assistance of an Apple IIe computer and the PAR 322 Softcorr software. Steps to potentials in both the active (-275 mV) and passive region (+750 mV) of the samples were investigated.

Surface analysis measurements were made in a Perkin-Elmer[f] Physical-Electronics 560 surface analysis system that had x-ray photoelectron spectroscopy (XPS), Auger electron spectroscopy (AES), and ion sputtering capabilities. Non-monochromatic Mg kα x-rays were used for the XPS measurements. XPS survey data were collected with a 100-eV pass energy, and multiplex data were collected at 25-eV pass energy. The binding energy scale was calibrated by adjusting the 3p and 2p3/2 photolines for clean copper to appear at 75.13 ± 0.02 and 932.67 ± 0.02 eV, respectively. Photoline peak areas, after inelastic background removal, were converted to atomic composition

[a]Johnson Matthey Inc., Malvern, PA.

[b]Implant Sciences Corporation, Danvers, MA.

[c]Battelle Memorial Institute, Columbus, OH.

[d]Fisher Scientific Co., Pittsburgh, PA.

[e]EG&G Princeton Applied Research, Princeton, NJ.

[f]Perkin-Elmer Corp., Physical Electronics Division, Eden Prairie, MN.

by the use of published sensitivity factors (10). The surface analysis system was connected to the electrochemical cell shown in Fig. 2 through the UHV transfer system that allowed a specimen to be transported to and from the spectrometer to the solution without exposure to air. Auger sputter depth profiles of corrosion layers were obtained using a 5-kV Ar ion beam rastered to give the desired sputter rate. The rate of sputtering was determined by measuring the time to remove a known thickness of SiO_2 from a silicon wafer. Auger data were collected in the EN(E) mode using a 5-kV incident electron beam.

A three-electrode system was used for all electrochemical measurements. The working electrode was the iron specimen under study; a platinum wire was used as the counter electrode; and the saturated calomel electrode (SCE) fitted with a Luggin probe was used as the reference electrode. All potentials reported in this work are with respect to SCE unless otherwise noted. Slight differences in procedures for specimens analyzed in a standard corrosion cell and those examined using the UHV transfer system are noted below.

Samples that were tested in the standard electrochemical cell (11) were spot-welded to a stainless steel connecting rod. The rod and part of the sample were masked with lacquer to allow a representative area of the sample to be exposed to the electrolyte. Exposure area varied from 0.2 to 1.0 cm^2, depending on the sample. Samples tested using the UHV/surface analysis system were spot-welded to a small stainless steel wire, which in turn was attached to the transfer device. No masking was applied in the UHV studies.

Once the nitrate solution was prepared, the argon or nitrogen sparging was stopped, an argon or nitrogen blanket was applied above the solution, and the working electrode sample was lowered into the electrolyte. For studies performed with the standard electrochemical cell, the sample was oriented vertically and completely submerged since the lacquer prevented exposure of undesired areas. For studies using the UHV system, the sample was lowered in a horizontal position so that it just touched the surface of the electrolyte. Surface tension effects minimized exposure of edges of the sample to the solution.

A few additional steps were applied to specimens used in the UHV transfer system. First, most specimens were placed into the spectrometer for analysis prior to electrochemical tests. Carbon and other contamination on the specimen surface were usually removed by a short ion sputter before the specimen was transferred to the corrosion cell. This step did not appear to have a significant influence on the electrochemical data for these samples. After polarization in the UHV transfer system corrosion cell, samples were rinsed with about 50 mL of deaerated deionized water upon removal from the electrolyte using the nozzle attachment shown in Fig. 2. After rinsing, each sample was flushed with a stream of nitrogen gas to remove water remaining on the sample. The sample was then raised into a chamber and vacuum pumping initiated. An initial liquid nitrogen cooled cryopumping stage was used to lower the pressure before the chamber was evacuated by a turbomolecular pump. When adequate vacuum was achieved the sample was moved to the spectrometer for analysis.

Experimental Results

Electrochemical Polarization

Potentiodynamic curves for pure iron and Fe-15P in deaerated 55 wt% $Ca(NO_3)_2$ at 60°C are shown in Fig. 3. Clearly, the presence of 15% phosphorus accelerated the corrosion of iron in both the active and passive regions, with the effect being more pronounced in the passive region. At -275 mV, the current density increased from 18 to 85 $mA \cdot cm^{-2}$ with the addition of phosphorus, while at +750 mV, the current density increased from 0.050 $mA \cdot cm^{-2}$ to 8.0 $mA \cdot cm^{-2}$. The open-circuit corrosion potentials observed in this work were -448 mV for pure iron and -550 mV for the amorphous alloy. These values are very close to those observed previously (9) for pure iron (-454 mV) and an alloy containing 2 wt% phosphorus (-558 mV). The addition of phosphorus appears to shift the open-circuit potential to more negative values.

Results of potential-step experiments on pure iron and Fe-15P, at -275 mV and +750 mV, were consistent with the potentiodynamic data. As shown in Figs. 4 and 5, after some transient behavior when the potential step was first applied, the current density in each case[a] settled to an apparent steady-state value. At -275 mV, this value was about a factor of 10 higher for Fe-15P than for pure iron; while at +750 mV, the current density was about three orders of magnitude larger with phosphorus present.

The results for the P-implanted samples, also shown in Figs. 4 and 5, appear, at first, very different from those for the amorphous alloys. At both -275 mV and +750 mV, the P-implanted specimens had a much larger initial current density than pure iron, but gave a smaller current density than that observed for Fe-15P. After about 10 s at -275 mV and 5 s at +750 mV, however, the current densities had fallen to levels identical to pure iron.

Integrating the area under the i versus t curves for the P-implanted samples indicated that sufficient charge was passed during the first 10 s at both -275 mV and +750 mV to corrode almost completely through the P-implanted region. At -275 mV, approximately 0.29 C was passed during the first 10 s after applying the potential step. Assuming a two-electron reaction for iron in the active region, this corresponds to the removal of a 210-nm layer of metal. Similar calculations for the +750 mV data gave approximately 0.3 C. Assuming a three-electron transfer in the passive region, this gives approximately 150 nm of corrosion. The positions A and B in Fig. 1 indicate these calculated amounts of metal removed

---

[a]The Fe-15P sample corroded very quickly at -275 mV, limiting the duration of the test to only 30 s. Consequently, reference to a measurement for this sample as "steady-state" is somewhat qualified.

on the P-implant profile. In both cases, the corrosion proceeded to a depth well below the phosphorus-rich region of the original sample.[a]

Clearly, the higher currents for the P-implanted samples can be ascribed to the corrosion of the phosphorus-containing outer region. The response was particularly rapid at +750 mV with most of the corrosion occurring in the first 1 s. The earliest data were collected in our studies were at about 0.1 s with current densities on the order of 1 $A \cdot cm^{-2}$. This value is consistent with current densities measured in the "passive" region for alloys with phosphorus concentrations close to 6.4 at.% (8), the estimated concentration of phosphorus in the surface layers of the P-implanted samples.[b] In both the active and the passive regions, after the corrosion has reduced the phosphorus in the metal phase to sufficiently low levels[c], the corrosion slows appreciably to a rate characteristic of pure iron.

Surface Analysis of Corrosion Products

The corrosion layers formed on samples of pure and P-implanted iron were examined with XPS after transfer from the corrosion cell to the spectrometer using the transfer system and procedures described earlier. Specimens were examined after 10 s and 300 s polarizations at potentials of -275 mV and +750 mV. Objectives of the analysis were comparison of the chemistries of the corrosion films at the two potentials and a determination of the differences in film chemistry caused by phosphorus. After collection of a survey spectrum for each specimen, multiplex spectra were collected for Fe 2p, Fe 3p, O 1s, P 2p, and C 1s photolines. Although only small changes in binding energy have been observed for different iron oxides, a good oxide data base exists and the current spectra are interpreted in light of the existing data. In particular, extensive use is made of work published by McIntyre and Zetarak (13), Brundle et al. (14), and Mills and Sullivan (15).

A collection of raw iron 2p N(E)/E data comparing different specimen types and conditions is shown in Fig. 6. Figs. 7 through 9 highlight differences between active and passive conditions and changes due to the presence of phosphorus using Fe 2p3/2, O 1s, and Fe 3p data. The compositions of the corrosion scales as determined by XPS peak areas are summarized in Table 1.

---

[a]Positions A and B are sufficiently deep within the sample that an estimated 20 to 30% uncertainty in the graphical determination does not seriously affect the conclusions.

[b]Similar rapid responses have also been observed during the polarization-induced mechanical abrasion of certain amorphous alloys (12). For example, current densities near 1 $A \cdot cm^{-2}$ have been estimated during the first 0.1 s for Fe-10Cr-13B-7P in 0.1 N H_2SO_4.

[c]"Sufficient" is used here in a qualitative sense. More precise determinations await the completion of higher-speed detection experiments currently under way.

Pure Iron Data. Relatively minor but significant differences were observed in the 2p and 3p spectra collected on pure iron at active and passive potentials as shown in Figs. 6 and 7. In particular, both the 2p3/2 and 3p spectra formed at -275 mV are broader than the corresponding spectra formed at +750 mV. The approximate peak position taken from the raw N(E)/E spectra for the 2p3/2 passive peak is 711.1 eV with a peak width of roughly 4.5 eV. This compares quite favorably with the data reported by Brundle et al. (14) for the Fe^{3+} peak in Fe_2O_3 and other compounds ($\approx$711.2 eV, 4.5 eV FWHM for Fe_2O_3, FeOOH, and Fe_3O_4). Because of this correspondence and because Fe_2O_3 is likely to form at passive potentials, we consider the film formed on pure iron at 750 mV to be made up mostly of Fe_2O_n. The 3p data are also consistent with this assignment. Our 3p data peak is centered at $\approx$55.8 eV, $\approx$3.4 eV FWHM. McIntyre and Zetarak indicate that the Fe^{3+} 3p peak is 55.7 eV with $\approx$3.5 eV FWHM.

A broadening of the iron 2p3/2 and 3p photolines with the addition of an Fe^{2+} component is also consistent with observations by McIntyre and Zetarak and Brundle et al. for Fe_3O_4. Brundle et al. observe that the Fe^{2+} peak appears to be located at $\approx$709.7 eV with $\approx$4.5 eV FWHM for Fe_xO and at $\approx$709.5 eV in Fe_3O_4. McIntyre and Zetarak found that the addition of an Fe^{2+} component added a peak at approximately 53.6 eV to the 3p peak. Without additional detailed analysis these data indicate that, for pure iron, mostly Fe^{3+} forms at passive potentials and that a mixture of Fe^{2+} and Fe^{3+} forms in the active region.

To provide a rough indication of relative amounts of Fe^{2+} and Fe^{3+}, the iron 2p3/2 spectra for several films, after background subtraction, were compared with computer-generated spectra based upon $\approx$3.8 eV wide pairs of photopeaks located at 710.8 (80%) and 714.0 eV ($\approx$20%) for Fe^{3+} and 709.7 eV (80%) and 712.9 eV (20%) for Fe^{2+}. The Fe^{3+} peak positions were initially based upon good fits to a passive film (Fe_2O_3) formed on iron in a borate buffer solution. Combinations of the two pairs of peaks could be adjusted to fit the pure iron spectra reasonably well. Fits to the Fe 2p3/2 spectra for phosphorus-containing layers worked well near the main peak, but an excess number of electrons were observed at binding energies $\approx$714 eV and higher. Approximate ratios of the 709.7 eV to 710.8 eV peak areas which appeared to fit the spectra reasonably well are reported in Table 1. Because of the overall complexity of the iron photospectra and additional complications due to the presence of phosphorus the exact ratios obtained from the fits should not be taken too seriously. However, the ratios support the views that mostly Fe^{3+} is present at passive potentials and that both Fe^{3+} and Fe^{2+} are observed at active potentials. Iron associated with the oxidized phosphorus appears to be primarily Fe^{3+}.

The oxygen spectra in Fig. 7 show no difference between the active and passive potentials. This is also consistent with data for the bulk oxides where the oxygen photolines were essentially independent of the oxide state. Note, however that the oxygen photopeak is not symmetric. This peak can most easily be fit with peaks located at roughly 530.2 and 531.7 eV. The largest peak at $\approx$530 eV is the oxide peak. The nature of a $\approx$531.7 eV-peak is subject to some debate. Often this peak is taken to indicate the presence of OH. In fact, a large peak at this energy is present for FeOOH (14). However, oxides grown in

a vacuum chamber in pure O_2 and bulk oxides with fresh surfaces exposed in an inert environment also show this peak (14). Therefore, the presence of OH will contribute to a peak in this location, but such a peak offers no assurance that OH is present.

The Influence of Phosphorus in the Active Region. Comparison of the Fe 2p data, Fig. 6, for pure iron at active potentials after 10 s and 300 s shows only slight differences. However, the comparable data for the P-implanted specimens shows significant changes in the Fe 2p peaks and related changes for the O 1s and Fe 3p spectra, shown in Figs. 6 and 8. At short times, both the Fe 2p3/2 and 3p peaks are narrower than those observed for the pure iron at active conditions. After the longer time the iron photopeaks get somewhat broader, similar to film formed on pure iron at these conditions. Initially the O 1s peak shows an enhanced signal at $\approx$531.7 eV, but with time this peak diminishes and the O 1s spectra begin to look like that observed for the pure Fe. Some indication of the cause of these changes is apparent in Table 1 where a significant concentration of phosphorus is observed to be in the film at short time and to decrease at the longer time.

Fig. 10 shows the AES depth profile of the film formed on the P-implanted specimen after the 10-s exposure at -275 mV. The boundary between the metal and metal oxide is probably uneven, given the polycrystalline nature of the product. This is supported by the irregular way in which oxygen shows variation as a function of depth into the film. If the film thickness is estimated by the drop in the oxygen signal to 50% of the maximum value or 50% of the plateau value, a thickness between 45 and 65 nm is obtained. The phosphorus occurred in two forms: as a reduced species (120 eV) and as an oxidized species (114 eV). The phosphorus located within the outer 10 nm of the surface gave an AES peak typical of oxidized phosphorus as found at the surface after either active or passive polarization occurred. Deeper within the scale, significant amounts of phosphorus in a reduced[a] state were observed. This species is designated "phosphide" or P^δ after Grabke et al. (9), who identified it on phosphorus-containing samples polarized in sulfate but not in nitrate solutions. Grabke et al. argued that the phosphide was oxidized to phosphate by nitrate before it could be detected by surface analysis. The current results support this conclusion for phosphorus occurring near the metal oxide-electrolyte boundary, but suggest that some P^δ may persist deeper within the corrosion product film. As discussed later, we believe that the P^δ occurs near the metal-metal oxide boundary, but may be distributed throughout the film because the boundary is rough.

The Influence of Phosphorus in the Passive Region. Comparison of the XPS photoline data for pure and P-implanted iron specimens after polarization at

---

[a]The positions of the XPS and AES peaks for phosphorus and various phosphides are very close, hence exact identification of the species is not possible. Because there is almost certainly some electron shift even for pure phosphorus as a surface species or when dissolved in iron, the species is considered to have at least a partial negative charge, δ-.

passive potentials shows variations of a somewhat different nature than found at active potentials. First, the layers formed on the P-implanted specimens contain oxidized phosphorus and the concentration does not diminish with time (Table 1). In addition, the general width of the iron 2p3/2 and 3p photopeaks formed with phosphorus present are generally as narrow or even narrower than those formed on pure iron at passive potentials. Comparison with the peaks formed on pure iron at active and passive potentials suggests that most of the iron is in the Fe^{3+} state. The O 1s photopeaks show the type of peak shape associated with the presence of phosphate.

As shown in Fig. 11, the AES sputter depth profile of the film formed on the P-implanted specimens after 10 s at +750 mV is very different from the depth profile observed for active polarization. As before, taking the metal-metal oxide boundary as the position where the oxygen peak drops to 50% of maximum value gives a film thickness of about 12 nm, or about one-fifth the thickness in the active region. The boundary also appears much more distinct in the passive region. The P^{5-} concentration appears to be maximum at the metal-metal oxide boundary. At positions closer to the metal oxide electrolyte interface, phosphate is predominant. Within the metal, the P^{5-} concentration generally decreases with distance from the metal surface, suggesting that the corrosion in the first 10 s was sufficient to consume most of the phosphorus in the implanted region. This is consistent with the earlier calculation and position B in Fig. 1 being on the "metal side" of the peak for phosphorus concentration.

Corrosion Product Film Composition. To obtain an indication of the makeup of the films, an atomic composition of the corrosion layers was calculated using peak areas and sensitivity factors; the results are shown in Table 1. In addition to the chemical information obtained from XPS peak shape and position analysis, atomic ratios provide some indication of film chemistry. Because quantification of transition metals can be complex and sensitivity factors are only approximate, the Fe sensitivity factor was adjusted until the Fe/O ratio for the passive film obtained after 10 s on pure iron gave the ideal Fe_2O_3 value of 0.67. As an indication of how much iron was associated with oxide and how much with phosphate, it was assumed that each phosphorus was associated with one iron atom and the remaining iron was associated with oxide. The Fe/O ratio with PO_4 removed was obtained by taking the iron associated with oxide {(Fe at.%) - (P at.%)} divided by the amount of oxygen not associated with PO_4 {(O at.%) - 4 x (P at.%)}.

It should be noted that the analyses undertaken suggest that the passive films are made up of iron in an Fe^{3+} state and that the active films generally involve Fe^{3+} and Fe^{2+}. An effort has been made to sort out the relative phosphate and oxide composition of the films. The analysis does not give evidence of FeOOH, but its presence at some level cannot be completely ruled out. Similarly, FeO_x may be present, but it is not directly resolved in the current analysis. The Fe^{2+}/Fe^{3+} peak ratio for the 300-s pure iron suggests more Fe^{2+} in the corrosion layer than can be accounted for in Fe_3O_4.

Several trends can be observed in Table 1. First, there is a greater amount of oxygen at higher potentials, consistent with a higher oxidation state as indicated above. Second, the amount of phosphorus in the films at active potentials decreases with time, while at passive potentials for up to 300 s the relative amount of phosphorus is nearly constant or grows slightly. Third, after the correction for PO_4, the Fe/O ratio at active potentials for pure and implanted specimens is nearly constant. The corresponding Fe/O ratio after correction at passive potentials is not as constant, but the major deviation occurs for the 300-s film where the amount of correction was very large.

Discussion

The Role of Phosphorus in Corrosion

Active Region. When pure iron corroded at active potentials in 55 wt% $Ca(NO_3)_2$ at 60°C, it gave mixed Fe^{2+}/Fe^{3+} corrosion products, presumably mostly Fe_3O_4. For the faster corroding P-implanted iron samples, the corrosion products were composed of an outer layer of $FePO_4$ and an inner layer likely to be Fe_3O_4 containing some P^δ. The two states of phosphorus suggest that phosphorus may accelerate the corrosion in either of two ways: (a) as P^δ at the metal surface or (b) as phosphate formed from P^δ within the corrosion product layer. While not ruling out (a), which appears to play the dominant role in the passive region (discussed later), the properties of the phosphates and the results of some additional experiments support (b) as an important factor in the active region.

Since the P^δ was not present in significant quantities close to the electrolyte, it appears that the P^δ reacted with a component of the electrolyte. Most likely, the P^δ was oxidized to phosphate by nitrate ions as proposed by Grabke et al. (9). This is supported by comparing the chemistry of phosphorus in nitrate and sulfate solutions. Current densities for pure iron and Fe-15P in 1 N Na_2SO_4 and pure iron in the nitrate solution were all similar (about 18 $mA \cdot cm^{-2}$) and very different from Fe-15P in the nitrate solution (85 $mA \cdot cm^{-2}$), indicating that the accelerating effect on corrosion caused by phosphorus in the active region requires the presence of the nitrate ion.

The thermodynamic properties of the phosphates suggest that their formation may facilitate the dissolution of iron during corrosion in the active region. The active region, specifically -275 mV, is on the negative-potential side of the peak potential for iron in hot nitrate solutions as shown in Fig. 3. Consequently, Fe^{2+}-containing reaction products should be important. In the case of the phosphates, $Fe_3(PO_4)_2$ should occur. Analysis of XPS data did not support the presence of significant amounts of $Fe_3(PO_4)_2$, at least in the outer layer of the corrosion product film. The data were interpreted to support the presence of $FePO_4$ instead. However, as shown in Fig. 12, the formation of $FePO_4$ is explained by comparing the potential-pH diagram for iron-phosphate with iron-phosphate in the

presence of nitrate.[a] While $Fe_3(PO_4)_2$ is stable at -275 mV (-0.034 mV vs. NHE) on iron in the presence of phosphate alone (16), $FePO_4$ is clearly more stable at this potential in nitrate solutions. Consequently, the following reaction with nitrate and $H_2PO_4^-$, the stable phosphate species at pH = 4.5, probably occurs sometime after $Fe_3(PO_4)_2$ forms.

$$2Fe_3(PO_4)_2 + 2H_2PO_4^- + 3NO_3^- + 2H^+ = \hspace{3cm} (1)$$

$$6FePO_4 + 3NO_2^- + 3H_2O$$
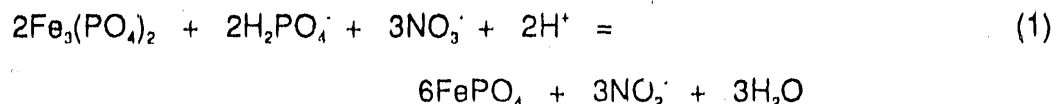
Despite the formation of $FePO_4$, $Fe_3(PO_4)_2$ may have been present close to the metal surface. In fact, in the presence of H_2PO^4, $Fe_3(PO_4)_2$ is strongly favored over $Fe(OH)_2$ at pH = 4.5. For the reaction

$$3Fe(OH)_2 + 2H_2PO_4^- + 2H^+ = Fe_3(PO_4)_2 + 6H_2O \hspace{2cm} (2)$$
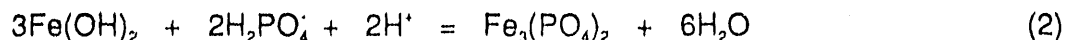
at pH = 4.5 and 25°C, assuming $[H_2PO_4^-]$ = 0.1 M, ΔG is -139 kJ.[b] $Fe_3(PO_4)_2$ is also quite soluble at pH = 4.5 according to Fig. 12.

Since $Fe(OH)_2$ is probably a precursor for the semi-protective[c] Fe_3O_4, the above considerations strongly suggest that the presence of phosphate facilitates the dissolution of iron in the active region by inhibiting the formation of the corrosion reaction film.

---

[a]Only reactions involving nitrate as an oxidizing agent were considered. The effects of nitrate on solubilities were not included in this diagram.

[b]Thermodynamic data were obtained from References 16 and 17.

[c]Recent electrochemical impedance data collected in our laboratories show negative impedance loops for pure iron polarized in the active region in hot nitrate solutions. These data support the existence of a film with some protective quality.

$$Fe \xrightarrow{\text{polarization}} Fe(OH)_2 \dashrightarrow Fe_3O_4 \text{ (film)}$$

$$+$$

$$P \dashrightarrow P^{5+} \dashrightarrow \underset{NO_3^-}{H_2PO_4^-}$$

$$\Big\downarrow H^{\cdot}$$

$$Fe_3(PO_4)_2 + H_2O$$

$$\Big\downarrow NO_3^-$$
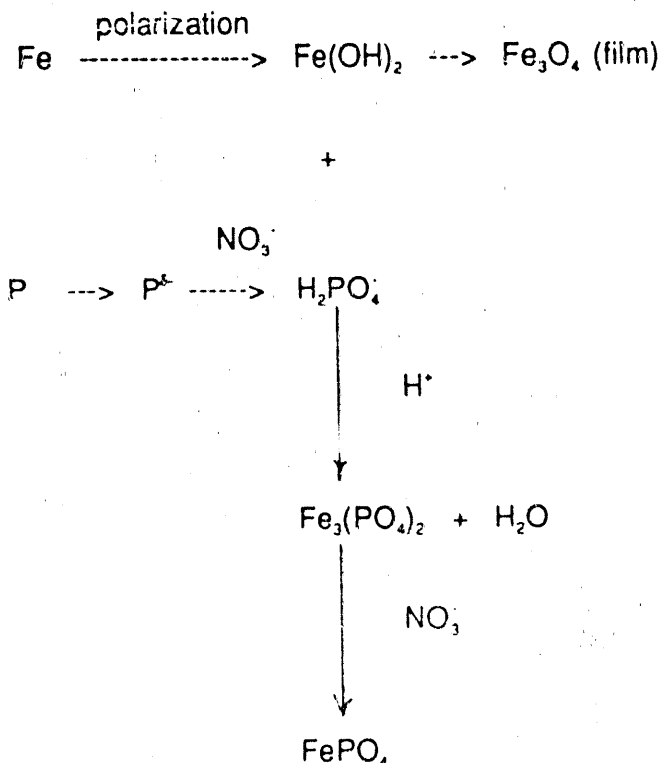
$$FePO_4$$

Nitrate is involved in the formation of the phosphate ion and, ultimately, $FePO_4$, both of which tend to shift the equilibrium away from the formation of Fe_3O_4. Nitrate is also known to facilitate the dissolution of $FePO_4$ (18), which would move the equilibrium further in the same direction.

Additional evidence for this mechanism is provided by polarization data for pure iron in dearated 55 wt% $Ca(NO_3)_2$ at 60°C with phosphate present. As shown in Fig. 13, when phosphate was present the current density was higher at -275 mV and the active region extended over a wider potential range. This suggests that phosphate contributes to active corrosion and supports the proposed reactions. Conversely, at passive potentials, the phosphate may inhibit corrosion.

Passive Region. The passive film formed on pure iron in 55 wt% $Ca(NO_3)_2$ at 60°C was composed primarily of Fe_2O_3. The presence of phosphorus accelerated corrosion, and the relative effect was more pronounced than in the active region.

The polarization data in Fig. 13 indicate that phosphate does not promote corrosion in the passive region, and thermodynamic calculations, similar to those considered for the active region, corroborate this finding. For example, the reaction

$$Fe_2O_3 + 2H_2PO_4^- + 2H^+ = 2FePO_4 + 3H_2O \qquad (3)$$

is disfavored, $\Delta G = +48.0$ kJ at pH $= 4.5$ and 25°C, again assuming $[H_2PO_4^-] =$ 0.1 M. This suggests that Fe_2O_3, once formed, is largely unreacted with the phosphate formed by the oxidation of P^{δ^-}. For the corresponding equation involving the hydroxide, $Fe(OH)_3$,

$$Fe(OH)_3 + H_2PO_4^- + H^+ = FePO_4 + 3H_2O \qquad (4)$$

the ΔG is $+1.9$ kJ under the same conditions. While the ΔG is positive for this reaction, it is comparatively small and the reaction is not strongly favored in either direction. Rather, it is close to equilibrium, suggesting $Fe(OH)_3$ and $FePO_4$ coexist in significant quantities. It is interesting that typical phosphate coatings used to protect steel surfaces are composed of a mixture of Fe_2O_3 and $FePO_4$, with the latter at concentrations around 35 wt% (18) which is not too different from concentrations measured in the passive film in this work. Recent work (16) has also suggested that hydroxylphosphates such as $2FePO_4 \cdot Fe(OH)_3$ form under conditions similar to those in this study. If these composite films did form in the nitrate solutions in this work, the hydroxylphosphates or their dehydrated analogs appear to have a passivating capacity similar to pure Fe_2O_3 formed in non-phosphorus containing systems.

Since the phosphate ion does not appear to accelerate corrosion at +750 mV, the P^{δ^-} species may do so directly. One possibility is that the P^{δ^-} on iron at +750 mV oxidizes to phosphate in the presence of water (without requiring nitrate) and that this reaction, by some unknown mechanism, lowers the activation energy for iron oxidation. Corrosion would proceed until the P^{δ^-} concentration was sufficiently reduced to permit passivation. This would happen very quickly after polarization for the P-implanted samples but never completely (over the duration of the test) for the Fe-15P alloy.

Relationship of Phosphorus Effects to IGSCC. This work directly relates to observations of phosphorus-induced IGSCC of iron in the calcium nitrate solutions (1,2). While this work does not fully explain the effect, it does indicate some factors that may contribute to the IGSCC behavior.

IGSCC was observed to increase dramatically in the presence of phosphorus at grain boundaries. Crack growth rates as high as 10^{-2} m·s^{-1} were observed in some cases (1). These rates are inordinately high, corresponding to roughly 30 A·cm^{-2} of corrosion current density assuming the crack growth is exclusively corrosion derived. Clearly, both chemical and mechanical factors are at work. The corrosion studies in this work, however, indicate that corrosion reactions do play an important role.

The phosphorus-containing iron specimens gave very high current densities when polarized at +750 mV where the IGSCC has been observed. This condition sets up the possibility for locally enhanced dissolution for phosphorus-rich grain boundaries. The results from P-implanted specimens suggest that the $P^\star$ species is responsible for the accelerated corrosion rates, probably involving its effect on the metal matrix and iron chemistry during its oxidation at passive potentials. The $P^\star$ probably plays a similar role at grain boundaries, accelerating corrosion momentarily (at the crack tip) until sufficient phosphorus has been depleted from the metal matrix to permit passivation. What was formerly the crack tip consequently becomes the crack wall. The presence of nitrate may provide additional solubility to the iron corrosion products, thus facilitating transport away from the crack tip with significant reduction in concentration polarization.

Taken together, these effects would clearly contribute to a phosphorus-enhancement of IGSCC in hot nitrate solutions as has been observed. Additional work is under way to quantify these factors more precisely and, for comparison, to evaluate others, including the effects of other grain boundary impurities such as sulfur, carbon, nitrogen, and boron.

Conclusions

The presence of phosphorus in iron specimens, both when alloyed in the amorphous state and when prepared by ion implantation, accelerated corrosion in the active and passive regions, with the effect more pronounced in the passive region. In both the active and passive regions, a $P^\star$ species apparently contributed to the observed high corrosion current densities. In the active region, the $P^\star$ was oxidized to phosphate which, in turn, appeared to assist the dissolution of the semi-protective Fe_3O_4. In the passive region, the oxidation of $P^\star$ accelerated corrosion directly. The $FePO_4$ that formed in the passive region did not inhibit passivation but, rather, was incorporated in the passive film. The results were found to be consistent with the high IGSCC rates observed for iron containing phosphorus segregated at grain boundaries.

Acknowledgment

References

(1)   R. H. Jones, B. W. Arey, D. R. Baer, and C. F. Windisch Jr., This Journal, in press.

(2)   R. H. Jones, B. W. Arey, D. R. Baer, and M. A. Friesel, Corrosion, in press.

(3) R. B. Diegle, C. R. Clayton, M. A. Helfand, Y. C. Lu, and N. R. Sorensen, This Journal, in press.

(4) M. J. Danielson and D. R. Baer, Corros. Sci., **29**, 1265(1989).

(5) P. Marcus and H. Talah, Corros. Sci., **29**, 455(1989).

(6) D. R. Baer and M. J. Danielson, J. Vac. Sci. Technol., **A5**(4), 1147(1987).

(7) R. H. Jones, M. J. Danielson, and D. R. Baer, J. Materials for Energy Systems, **8**, 185(1986).

(8) J. Kupper, H. Erhart, and H. J. Grabke, Corros. Sci., **21**, 227(1981).

(9) H. Krautschick, H. J. Grabke, and W. Diekmann, Corros. Sci., **28**, 251(1988).

(10) C. W. Wagner in Practical Surface Analysis, ed. by D. Briggs and M. P. Seah, John Wiley & Sons, Chichester, 1983, p. 511.

(11) 1980 Annual Book of ASTM Standards, Part 10, G-5, American Society for Testing and Materials, Philadelphia, PA.

(12) K. Hashimoto and T. Masumoto, "Corrosion Properties and Amorphous Alloys," Chap. 8, from Glassy Metals: Magnetic, Chemical, and Structural Properties, Editor: R. Hasegawa, CRC Press, Inc., Boca Raton, FL, 1983.

(13) N. S. McIntyre and D. G. Zetanak, Analytical Chem. **49**, 1521 (1977).

(14) C. R. Brundle, T. J. Chaung, and K. Wandelt, Surf. Sci. **68**, 459 (1977).

(15) P. Mills and J. L Sullivan, J. Phys. D: Appl. Phys., **16**, 72ɔ (1983).

(16) T. Kodama, Boshoku Gijutsu, **23**, 545(1974).

(17) M. W. Chase, JANAF Thermochemical Tables, Third Edition, American Chemical Society and American Institute of Physics, New York, NY, 1986.

(18) L. L. Shreir, Corrosion, Vol. 2, Chap. 16.2, Newnes-Buttersworths, London, 1976.

Table 1. Surface composition of Fe and P-implanted (Fe-P) Electrode Surfaces

Sample		Atomic % and Atom Ratios					Thickness	Fe^{2+}/Fe^{3+}
	Fe	O	P	Fe/O	PO_4/Ox	Fe/O[*]	nm[+]	2p3/2 Peak Fit[**]
Fe Active 10 s	47	53	-	0.89	-	0.89		0.51
Fe Active 300 s	47	53	-	0.90	-	0.90		1.2
Fe-P Active 10 s	38	57	4.9	0.66	0.15	0.87	65	LT 0.09
Fe-P Active 300 s	44	54	1.6	0.82	0.04	0.90	260	0.38
Fe Passive 10 s	40	60	-	0.67	-	0.67	9.6	-
Fe Passive 300 s	40	60	-	0.69	-	0.69		LT 0.06
Fe-P Passive 10 s	26	65	9.2	0.40	0.55	0.60		-
Fe-P Passive 300 s	27	62	11	0.43	0.74	0.94	11.5	0

[*] PO_4 removed as discussed in text
[**] Based upon areas of 709.7 eV and 710.8 eV peak fits
[+] Based upon AES depth profiles
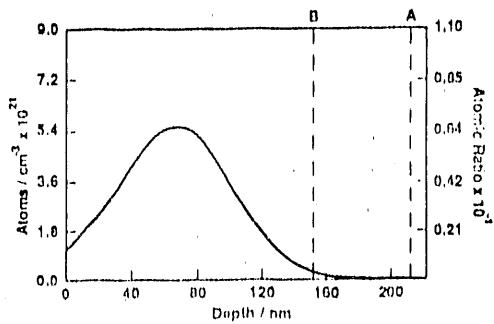
Fig. 1. Profile of phosphorus
concentration in the surface
region of ion-implanted
samples.
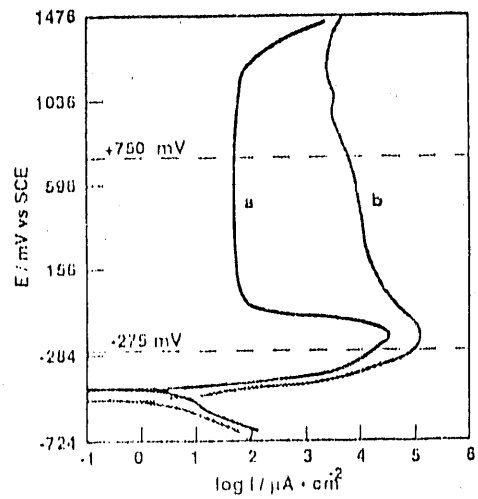
Fig. 3. Electrochemical
polarization curves for (a)
pure iron and (b) Fe-15P
alloy in 55 wt% $Ca(NO_3)_2$
at 60°C.
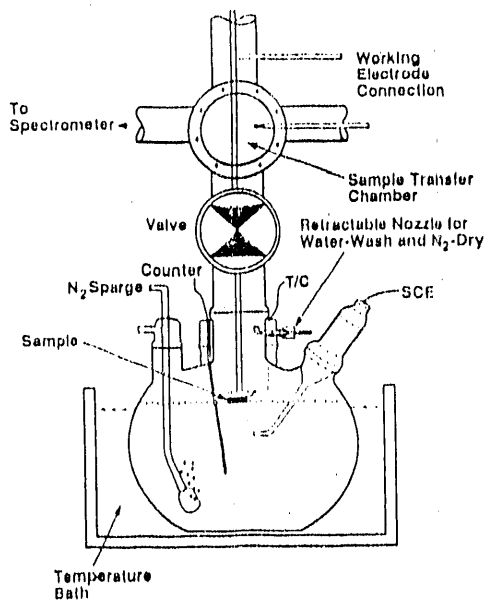
Fig. 2. Electrochemical cell
in UHV transfer system.
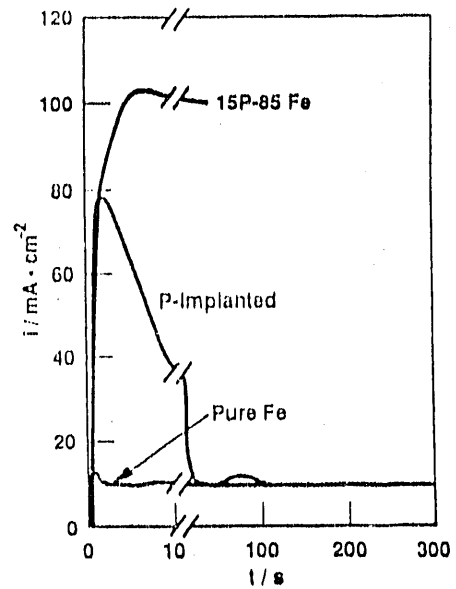
Fig. 4. Variation of current
density with time after
potential step to -275 mV.
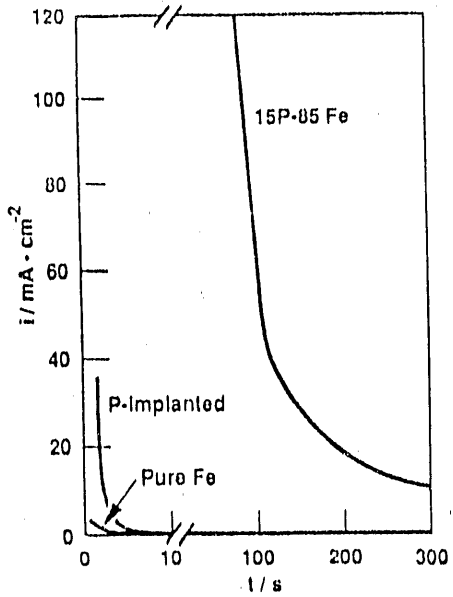
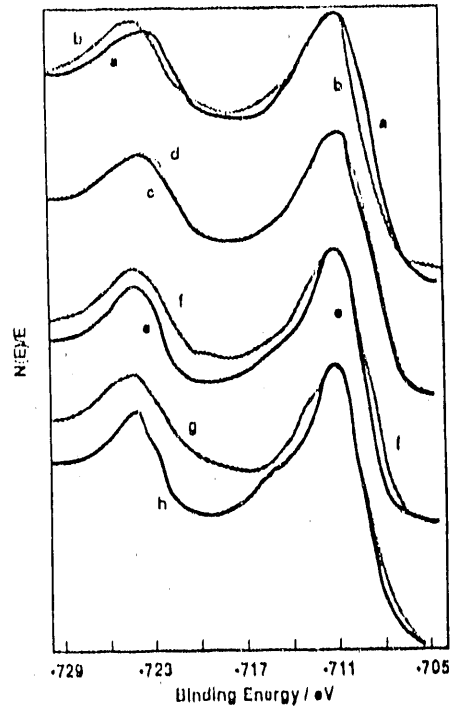Fig. 5. Variation of current density with time after potential step to +750 mV.

Fig. 6. Fe 2p XPS spectra for (a) pure Fe after 300 s at -275 mV, (b) pure Fe after 300 s at +750 mV, (c) pure Fe after 10 s at -275 mV, (d) pure Fe after 300 s at -275 mV, (e) P-implanted Fe after 10 s at -275 mV, (f) P-implanted Fe after 300 s at -275 mV, (g) pure Fe after 300 s at +750 mV, and (h) P-implanted Fe after 300 s at +750 mV.
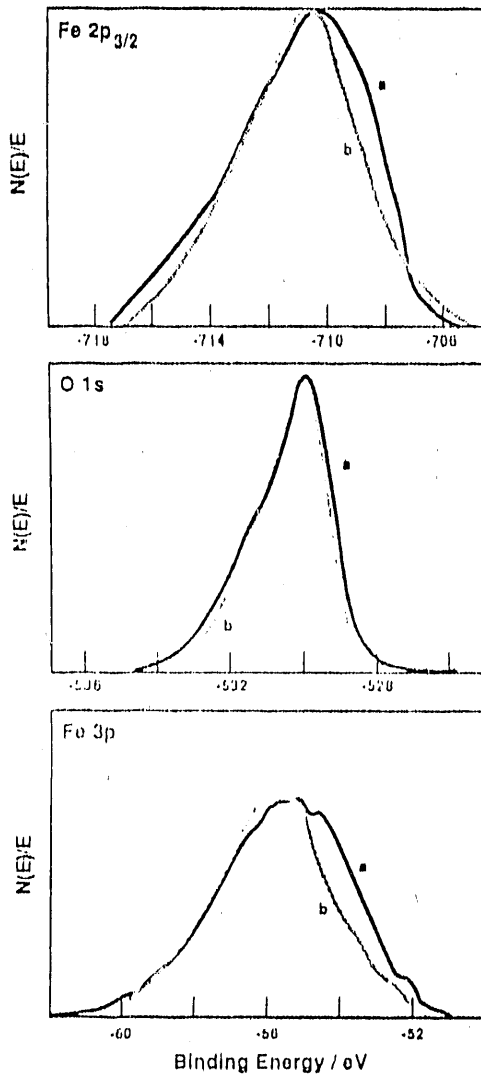
Fig. 7. Fe $2p_{3/2}$, O 1s, and
Fe 3p XPS peaks[2] for pure Fe
after 300 s at (a) -275 mV
and (b) +750 mV.
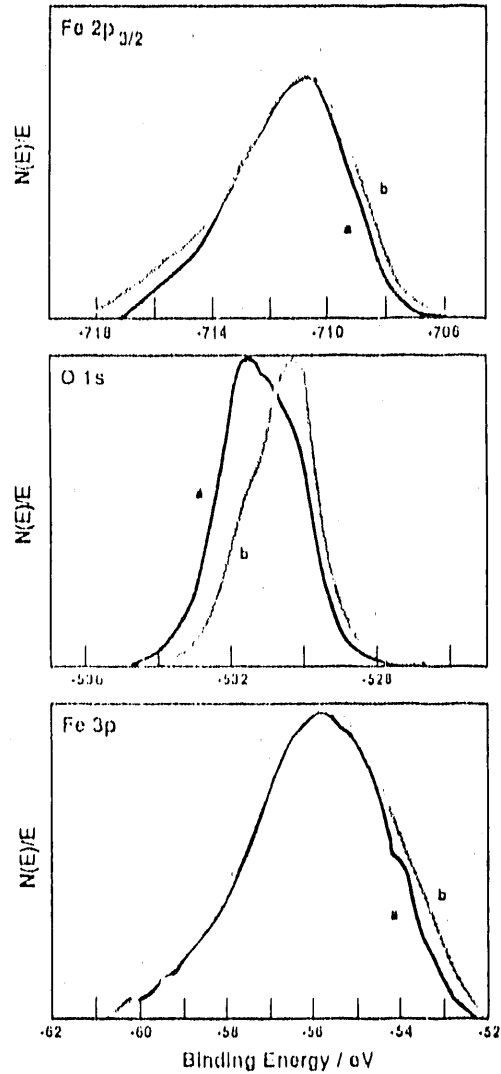
Fig. 8. Fe $2p_{3/2}$, O 1s, and
Fe 3p XPS peaks[2] for P-
implanted Fe after (a) 10 s
and (b) 300 s at -275 mV.
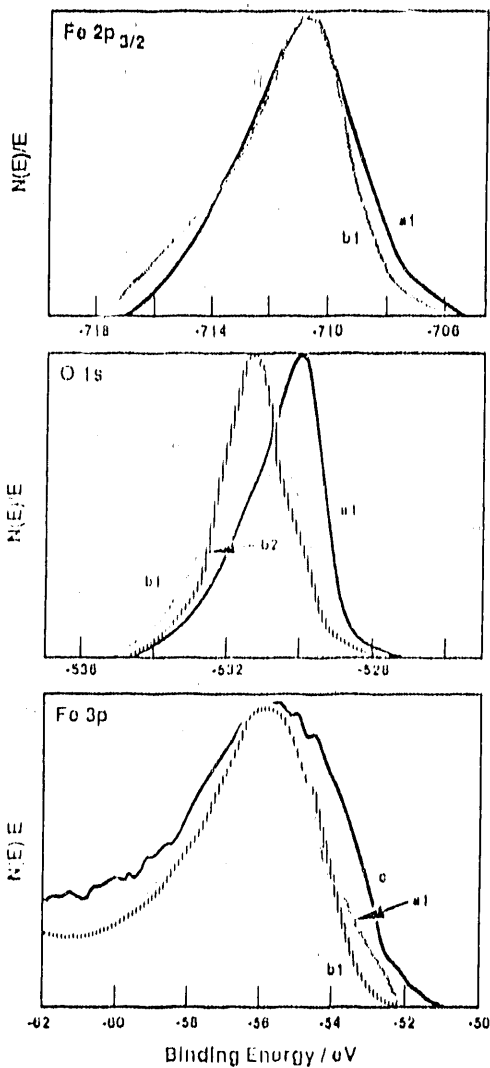
Fig. 9. Selected Fe $2p_{3/2}$, O 1s, and Fe 3p XPS peaks for (a1) pure Fe after 10 s at +750 mV, (b1) P-implanted Fe after 10 s at +750 mV, (b2) P-implanted Fe after 10 s at +750 mV, and (c) pure Fe after 10 s at -275 mV.
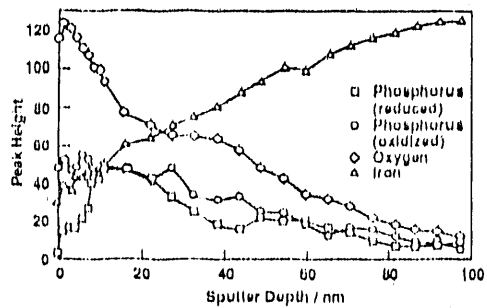

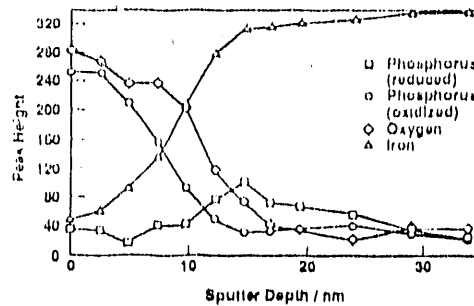Fig. 10. AES sputter depth profile for P-implanted Fe after 10 s at -275 mV.

Fig. 11. AES sputter depth profile for P-implanted Fe after 10 s at +750 mV.
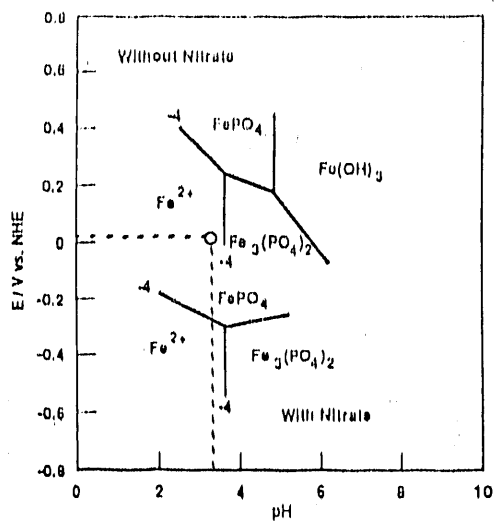
Fig. 12. Potential-pH diagram
for iron-phosphorus-water with
and without nitrate. Solubility
reactions involving nitrate are
not considered. $[H_2PO_4^-] = 0.1$ M

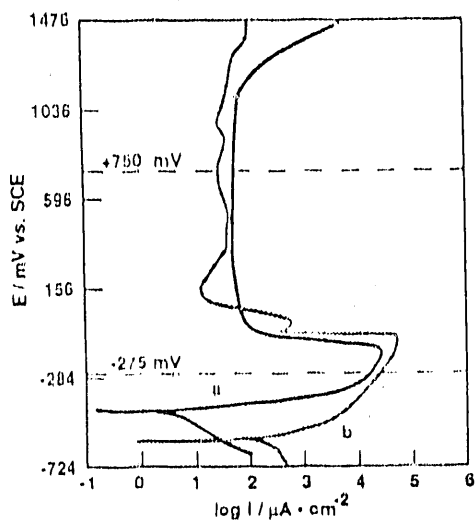Fig. 13. Electrochemical
polarization curves for pure Fe
in 55 wt% $Ca(NO_3)_2$ at 60°C (a)
without and (b) with phosphate
present.

END

DATE FILMED

12/18/90